MISSOURI S&T

15 Apr 2004, 7:00pm - 8:30pm

A Case History of the Use of Geofoam for Bridge Approach Fills

Armin W. Stuedlein
Geofoam Research Center, Syracuse, New York

Dawit Negussey
Geofoam Research Center, Syracuse, New York

Michael Mathioudakis
New York State Department of Transportation (NYSDOT), Albany, New York

Follow this and additional works at: https://scholarsmine.mst.edu/icchge

Part of the Geotechnical Engineering Commons

Recommended Citation

A CASE HISTORY OF THE USE OF GEOFOAM FOR BRIDGE APPROACH FILLS

Armin W. Stuedlein
Geofoam Research Center
Syracuse, New York-USA-13244

Dawit Negussey
Geofoam Research Center
Syracuse, New York-USA-13244

Michael Mathioudakis
NYSDOT
Albany, New York-USA-12232

ABSTRACT

A new bridge replaced the Route 85 Bridge over Normans Kill Creek in Albany, NY in 2001. The old bridge was a double span steel truss bridge with pile-supported abutments and a mid pier in the creek channel. The replacement is a single span concrete girder bridge and was constructed adjacent to the old bridge to minimize the extent of realignment of the roadway centerline. The soil stratigraphy along the creek bank consists of weak and compressible lacustrine deposits. During construction of the new bridge, the old bridge had to remain in operation. EPS geofoam was used as a lightweight substitute for soil to construct the approach fills for the new bridge to assure stability and minimize settlements. Extensometers and earth pressure cells were installed to monitor the performance of the approach fills. The roadway profile has been surveyed periodically to develop the settlement profile over time. In addition to improving stability and reducing settlements, the use of geofoam for the bridge approaches has resulted in additional benefits. The construction was quick and took place in winter. Lateral pressures against the abutments and wing walls are low. Results of the field monitoring are presented and compared with computer modeling of a representative section.

INTRODUCTION

Route 85 is a major arterial connecting south and west residential communities to Interstate 87 and Interstate 90 in Albany, NY. North of the Normans Kill Creek, Route 85 is designated as a primary highway, and as a secondary highway south of the creek. The original crossing had a northeast-southwest alignment (hereafter referred to as north-south) and was built in 1966. The bridge was a two-lane, two span steel girder bridge with a mid-pier in the creek channel. The Normans Kill Creek is a fast-rising and potentially aggressive creek flowing west to east, draining an approximately 400 km^2 watershed. The normal creek flow fluctuates about a mean elevation of around 28.5 m, while the 50-year design flood elevation is estimated at 35 m. The project location is shown in Fig. 1. There have been several areas of slope instability along the banks of Normans Kill Creek and tributaries.

Driving of concrete piles for the old bridge south abutment triggered slope movement. Consequently, low volume displacement H piles were used for support of the old north abutment. The south and north abutments carried the bridge deck and retained the grade supported compacted approach fill and overlying pavement structure. By 1970, the abutments showed early signs of distress. Subsequent inspections over the years showed rotation of the rocker bearings at the mid-pier and abutments, spalling of concrete at the mid-pier and the bridge deck. The poor bridge condition and increasing traffic volume required careful consideration of three rehabilitation and reconstruction alternatives. The first alternative considered a rehabilitation of the existing structure with no traffic improvement. The second alternative considered rehabilitation with widening to add a third lane. The third option was to construct a new three-lane bridge adjacent to the existing structure on a new centerline. Due to the existing high traffic volume, the selected alternative was required to maintain service on Route 85 during construction. The third alternative featuring construction of a new bridge while the old bridge remained in service was chosen. At completion of construction, traffic transferred to the new bridge and the old bridge was then demolished. Construction had to move quickly and carefully so as not to aggravate the distressed state of the existing bridge. To reduce the extent of construction and need for additional right-of-way, the new and old bridge centerline alignments were set as close as possible.

PROJECT DESCRIPTION

Steel H-piles were selected to support all of the new bridge abutments and wing walls. Sheet piles were driven adjacent to the east shoulder of the existing bridge approach, to enable excavation of the existing side slope and subgrade preparation for the new substructure. To mitigate potential scour damage, the mid-pier supporting a two span system was removed, requiring the abutment locations to move closer together. Fill heights required to reach the design grade were estimated at over 6 meters. Stability analyses subsequently indicated construction of the proposed approach fills in one stage may trigger movement. Excessive settlements were anticipated behind the abutments and the adjacent existing bridge over the

construction period. The most innovative aspect of the new bridge construction was the use of EPS geofoam for support of the approach pavement. The selection of geofoam as the approach fill material mitigated expected settlements and stability concerns. As a further benefit, the use of geofoam allowed for a reduction in lateral stress transfer and downdrag loading on the abutments and supporting piles.
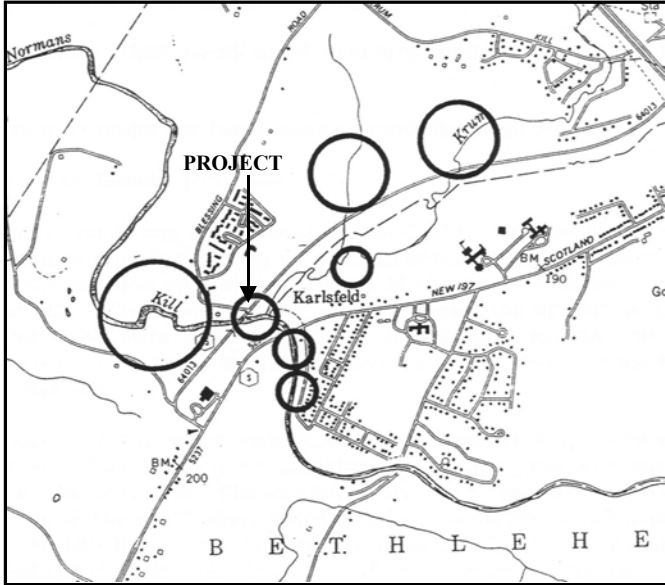

Fig. 1. Project location map for the Route 85 crossing. Circled areas show locations of previous landslide activity.

A total of 3000 m³ of EPS geofoam was used for the project, of which 1500 m³ was placed in the north approach. The Geofoam Research Center (GRC) in collaboration with the New York State Department of Transportation (NYSDOT) installed sensors within the north approach fill and established survey monuments on the edge of the roadway. The objective of the instrumentation program was to observe stress developments at various locations within the approach fill and to monitor settlements with time. The monitoring program began with construction of the north approach and continues to date. The observations will be useful if and when a matching twin bridge needs to be constructed and for calibration of numerical models.

SUBSURFACE CONDITIONS

The general soil profile developed from a series of borings by NYSDOT is summarized in Table 1. The boreholes along the creek channel penetrated to depths of 30 m and to minimum elevation of -10 m. All boreholes terminated in varved soft to stiff glacio-lacustrine silty-clay. Atterberg limit tests on recovered samples of the silty-clay indicated mean values for plastic and liquid limits of 20 and 35, with mean natural moisture content of 37 percent.

Table 1. Generalized soil profile at the Route 85 project site.

Depth (m)	Soil Description
0-2	Loose to compact brown sandy GRAVEL
2-7	Soft to very soft gray clayey SILT with layers of CLAY
7-20	Very soft to stiff varved silty CLAY with clayey SILT
20-23	Medium soft to stiff varved silty CLAY with clayey SILT
23-30	Stiff to firm varved silty CLAY with clayey SILT

APPROACH SYSTEM

The geofoam treated portion of the north approach is approximately 13 m wide and extends from station 36+995 to 37+450. Both abutments are aligned at 45° with respect to the roadway centerline and the north approach required substantially less excavation than the south approach. The limits of the north approach are shown in plan in Fig. 2.

Construction of the north approach fill began with installation of a combination of sheet piling and soldier piles and lagging along the east edge of the existing roadway. This allowed removal of portions of the then existing approach side slopes to construct the new abutment and wing walls. Thereafter, a 0.6 m layer of free draining granular bedding was placed in mid January 2001 as a leveling course for the geofoam fill. EPS 19 geofoam blocks, as per the newly adopted ASTM D 6817 and Type VIII as per ASTM C 578, having 0.9 by 1.2 by 2.4 m dimensions were placed in three layers to a height of 2.7 m. A 1.2 m wide fine to medium sand was placed and compacted in layers to form a perimeter chimney drain along the abutment and wing wall interfaces with the geofoam fill. Another three layers of geofoam and 2.7 m additional chimney drain fill was placed for a total fill height of 5.5 m. The chimney drain rests on the heel of the abutment and wing wall footings above a layer of crushed rock base drain, as shown in Fig. 3. All geofoam placement and installation of the chimney drain interface was completed within a week and at a time of freezing temperatures and snow cover. The geofoam fill was capped by a 100 mm thick reinforced concrete load distribution slab. The slab was poured directly over the geofoam surface. Construction drawings indicate the load distribution slab terminates at the edge of the geofoam fill. However, in the actual construction, the load distribution slab straddles across the chimney drain on to the retaining structures; abutment, wing walls and soldier piles. The load distribution slab also serves as protective cover for the geofoam against potential spillage of deleterious fluids, if ever necessary. Select fill and crushed rock, each of about 0.6 m thickness, constitute the sub-base and base for the 305 mm thick PCC approach slab and asphalt concrete pavement. The edges of the concrete slab rest on the abutment and wing walls. There is no self-evident rationale for providing the chimney drain system. The sheet pile and lagging between the old and new approach fills has been left in place.
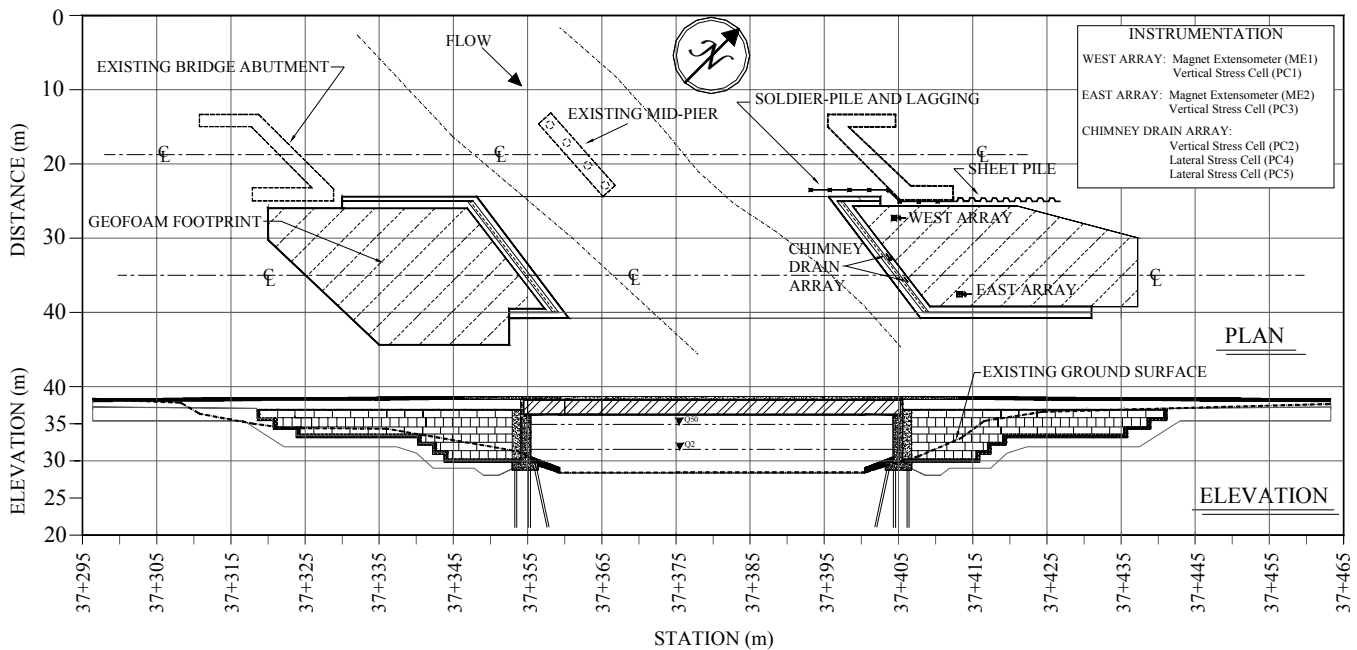
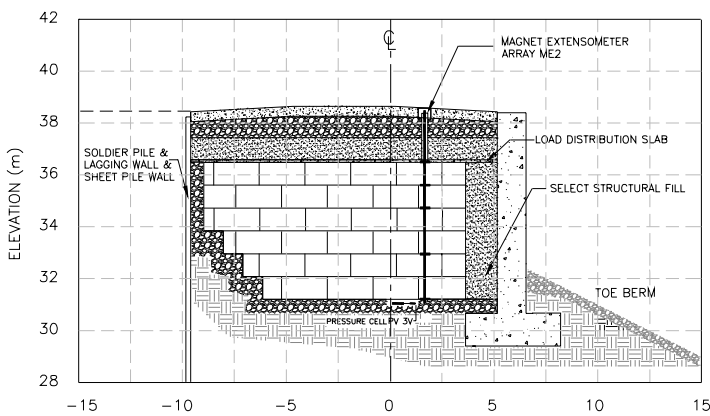*Fig. 2. Plan view of north approach and instrument locations.*

Fig. 3. Section through wingwall and sheetpile, elevation view of North approach fill showing the East magnet extensometer array basal stress cell.

Conventional compacted soil fill for constructing the approach system over the foundation soils and in close proximity of the existing bridge would have been difficult, as described above. Use of EPS geofoam in place of soil allowed close alignment of the old and new bridge centerlines without inducing further detrimental settlements and distress to the existing bridge. The use of geofoam was also recognized to reduce the overall construction time, equipment and truck traffic.

INSTRUMENTATION

Instrumentation and observations employed at the Route 85 geofoam approach include stress cells, magnet extensometers, and optical settlement surveying. Stress cells have been used at various geotechnical projects (O'Rourke, 1978; Munfakh, 1983; and Arai, 1996) and guidance on behavior of stress cells in soil media is provided by Weiler and Kulhawy (1978). The stress cells employed at the Route 85 project are of the pneumatic type and continue to be monitored with a nitrogen-gas supply and digital readout unit. The total stress cells are of 700 kPa maximum capacity, with an accuracy and resolution of +/- 0.2 kPa and +/- 0.1 kPa, respectively. Stress cells of lower capacity would have been preferred to monitor an application such as EPS lightweight fills, however, due to time limitations with construction scheduling, the readily available larger capacity cells were used. The manufacturer of the pneumatic stress cells supplied calibration data. Leads for the stress cells were run to the east wing wall and through a weep hole. A locking steel junction box was used to secure the leads outside the wing wall. Five stress cells were placed within the approach fill system. Two stress cells were placed in close proximity to the magnet extensometer columns (described below) as shown in Fig.'s 2 and 3, labeled PC1V and PC3V (the "V" indicating registration of vertical pressures). These cells were placed directly below the geofoam base in a pocket of medium sand within the gravel blanket drain. Another three stress cells were placed within the chimney drain separating the EPS geofoam from the abutment. Stress cell PC2V is placed at the base of the chimney drain; stress cells PC4H and PC5H are placed 0.6 m and 2.4 m above the base of the chimney drain and register horizontal pressures.

Magnet extensometers have been used to monitor settlements (Saye, et al., 2001; O'Rourke and O'Donnell, 1997). Magnet extensometer systems consist of a sensor probe, a graduated measuring-tape, a tape reel with built-in light and buzzer, and permanent magnets positioned along the length of an access pipe (Slope Indicator, 2002). The stainless steel probe, having dimensions 16 mm diameter by 203 mm length, is attached to 30 m long conducting wires embedded in the measuring tape and laminated in protective plastic The tape is marked in graduations of 0.01 ft and 1 mm on opposite sides. The manufacturer suggests that readings are repeatable to +/- 3 to 5 mm or +/- 0.1 to 0.2 inch. Conventional magnet plates are 305 mm square with a thickness of 13 mm and are of PVC. These

plates were used to monitor geofoam fills at the Interstate-15 reconstruction project and may have contributed to exaggerated settlements (Negussey, et al., 2001). However, the plates used for the R85 project consist of low profile galvanized steel magnet plates of the same 305 mm square dimensions but with a thickness of only 3 mm, shown in Fig. 4. These improved settlement plates represent a four-fold decrease in thickness so as to moderate stress concentrations and initial deformations at the magnet plate to geofoam block interfaces. A gas-powered augur was used to bore through successive geofoam blocks to facilitate passage of the 25 mm ID PVC riser pipes. Magnet plates were slipped over the riser pipes to selected positions within the approach fill. Magnet plates were placed at Level 0, between the gravel blanket drain and the first layer of geofoam, at Level 2, between the second and third geofoam blocks, and Levels 4, 5, and 6. A double casing system consisting of a 100 mm PVC riser pipe and a monitoring well casing was used to raise the PVC riser pipe to the road grade while protecting the geofoam fill from deleterious infiltrating liquids. Two magnet extensometer arrays were installed, ME1 and ME2, corresponding to the West Array and East Array, as shown in Figure 2.

Survey points were established along two profiles on the wearing surface of the Route 85 Crossing to monitor long term settlements. Survey readings were taken with a digital auto-level. This instrument uses a foldable staff marked with both a metric scale and a bar code. The standard deviation on 1 km of double leveling is 1.0 mm for the bar code staff and 1.5 mm for the metric staff (corresponding to electronic and visual measurement, respectively). Elevations can be read to 0.1 mm. Both instruments rely on a Charge Couple Device (CCD) comparable to that used in video cameras. The CCD acquires an image of the demarcations on the bar-coded staff. An internal correlation procedure calculates a rod reading and distance to the rod value from the analog video signal (Druss, et al., 1998).
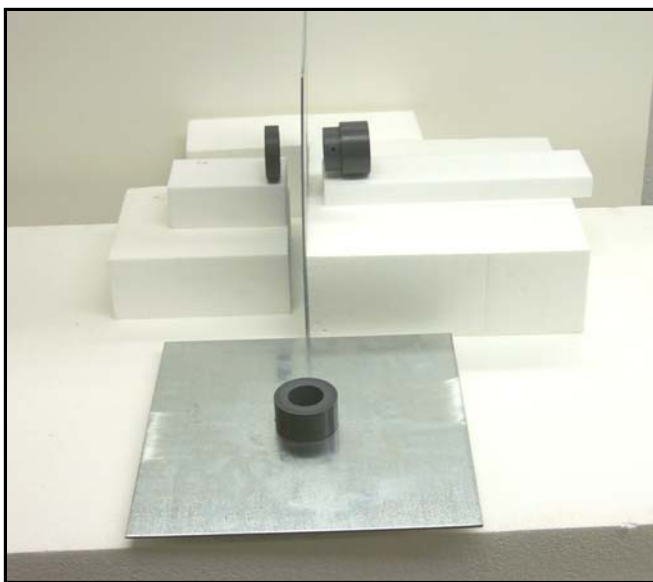

Fig. 4. Modified magnet plates used at the Route 85.

CONSTRUCTION AND LOADING TIMELINE

Construction of the Route 85 replacement bridge began in August of 2000. Since placement of geofoam fill does not require compaction, construction continued into winter. This had extra benefit in limiting runoff and silt loading from the construction site on to the creek channel. The south approach was raised to pavement elevation by December 2000. By January 2001, the north approach was ready for geofoam filling. Geofoam placement of the north approach began on 16 January, and was completed by 23 January. The load-distribution slab (LDS) was poured on 9 February. The pavement subbase was placed and compacted on 14 February. In preparation for the placement of the steel bridge girders, the contractor placed a 600 mm gravel pad on top of the subbase on 10 March. This was subsequently removed on 1 April, and the road-base was placed on 22 May. On 24 May, the approach slab was poured, comprising the last static load application to the portion of the geofoam fill that was instrumented. Asphalt paving began in June and ended on 31 July. Figure 5 shows the construction sequence graphically with the estimated surcharge load history. Total time for construction of the north approach was about 200 days, and included winter construction. The entire project was completed within a year.
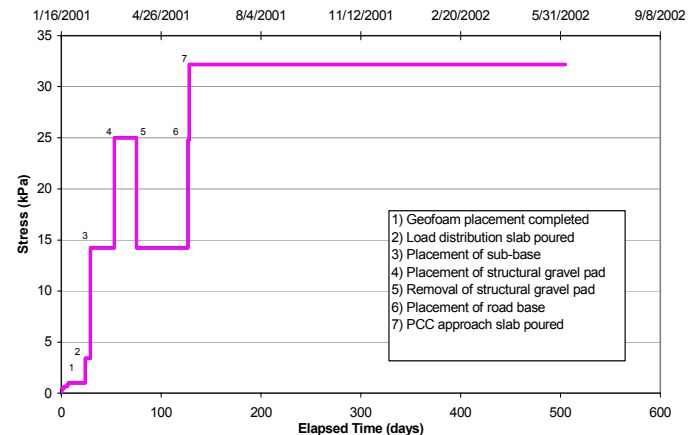

Fig. 5. Construction sequence and load history of the Route 85 north approach fill.

FIELD OBSERVATIONS

Following the two-stage installation of geofoam blocks and the chimney drain, baseline readings at Route 85 occurred after placement of the LDS. The extensometer settlement history of the geofoam fill is shown in Figures 6 and 7, for the East and West Array, respectively. Total construction-related settlements over the height of the geofoam fill are 30 and 27 mm for the East and West Array, respectively. The geofoam strains corresponding to construction settlements are about 0.5 and 0.6 percent for the East and West Array. The post-construction settlement time history spans a period of about 600 days. The frequency of observations has decreased with the opening of the road for service.

Total fill settlements increased to 45 mm for both arrays, corresponding to 0.8 percent strain. Both in trend and magnitude, the observed settlements at the East and West array are in good agreement.
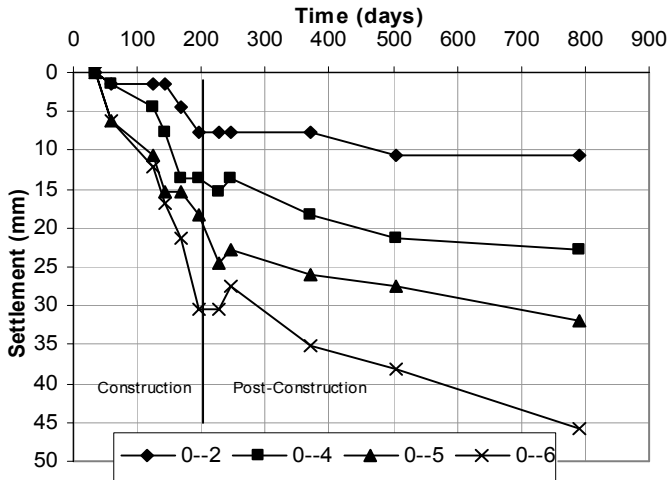

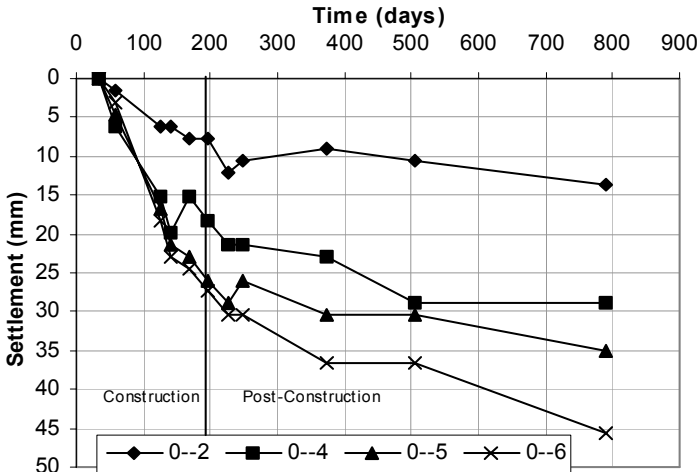*Fig. 6. Settlement of the geofoam approach fill, East Array.*

Fig. 7. Settlement of the geofoam approach fill, West Array.

The optical settlement surveys conducted after the end of construction are shown in Fig. 8. In the first year after construction, settlements of less than 10 mm occurred in the geofoam area gradually increasing as the profile transitions from geofoam to conventional fill section. The latest settlement survey indicates an increase in settlement in the geofoam treated area. Geofoam settlement of about 10 mm occurred over the time interval between the last two surveys., This settlement increment is reasonably consistent with corresponding magnet extensometer movements from 500 to about 800 days of the full thickness of geofoam fill, lines representing Levels 0-6.

The base stress cell readings and estimated load levels on the geofoam approach fill are shown in Fig. 9. Both base stress cells show under-registration of vertical pressures. Some portion of the load due to the overburden may be transferred from the LDS to the abutments and wing walls. Stresses
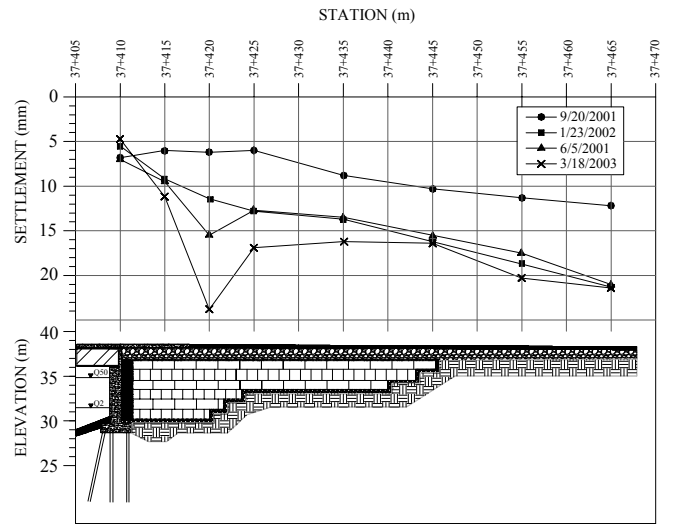
Fig. 8. Profile settlement survey along east edge of approach.

observed from cells placed in the chimney drain are shown in Fig. 10. The estimated pressures do not consider interaction between the fill and the walls and significantly overestimate vertical stresses. The separation between the abutment and geofoam fill is small and thus interaction effects are likely significant. Soil arching may be producing up to 60 percent reduction in vertical stresses at the base of the abutment by the end of construction. Horizontal stresses also attenuate by soil arching action. Equation (1), as suggested by Handy (1985) for estimation of maximum lateral earth pressures for "bin-effect" conditions gives values that are in reasonably good agreement with observations.

$$\sigma_{h,\,max} = \frac{\gamma B}{2\mu} \qquad (1)$$

where: γ = unit weight of backfill
  B = width of "bin"
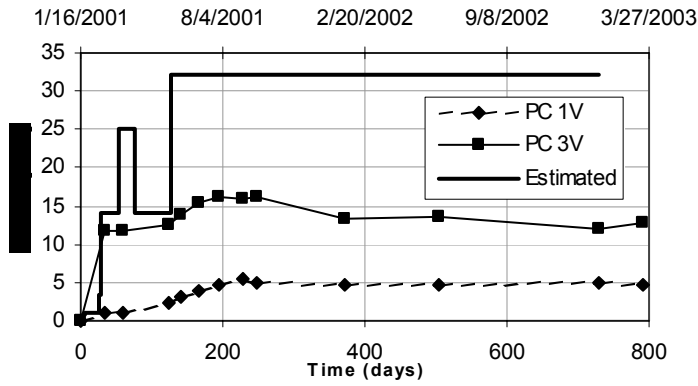 μ = coefficient of interface friction, $\tan(\phi_\iota)$

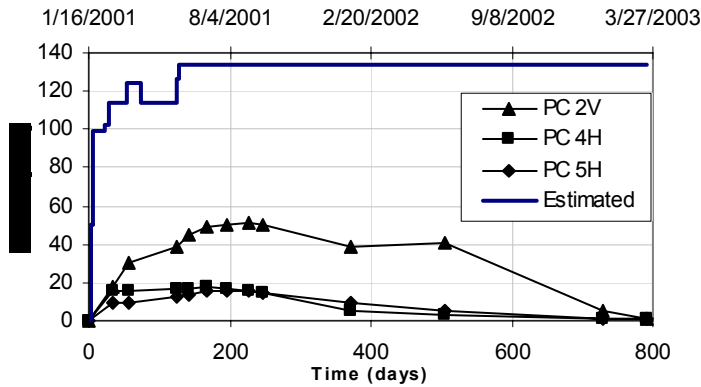*Fig. 9. Observed vertical stresses and estimated load history below geofoam approach fill.*

Fig. 10. Observed stresses and estimated load history at base of chimney drain.

Maximum lateral pressures of 17.5 and 15.8 kPa were registered by PC4H and PC5H (Fig. 10) and Stuedlein (2003) indicates close agreement with maximum lateral pressure estimates based on equation 1. The arching effect also moderates the vertical stress intensity as is evident from comparing PC2V and the geostatic stress estimate shown in Fig 10.

NUMERICAL MODELING OF GEOFOAM FILL

A series of numerical models based on a section perpendicular to the mid point of the abutment from Fig. 2 were run using FLAC (Fast LaGrangian Analysis of Continua) software. The models used interface elements, suitable constitutive models, and large strain computation. The model grid used about 4500 elements, shown Fig. 11. Material types and boundaries for the model are shown in Fig. 12. Numerical modeling of the site followed the actual stages of construction: (1) placement of geofoam and chimney drain behind the abutment, (2) addition of the LDS, (3) placement of pavement sub-base, (4) addition of pavement base, and (5) placement of PCC pavement. The material parameters and constitutive models used in the FLAC model are presented in Table 2.
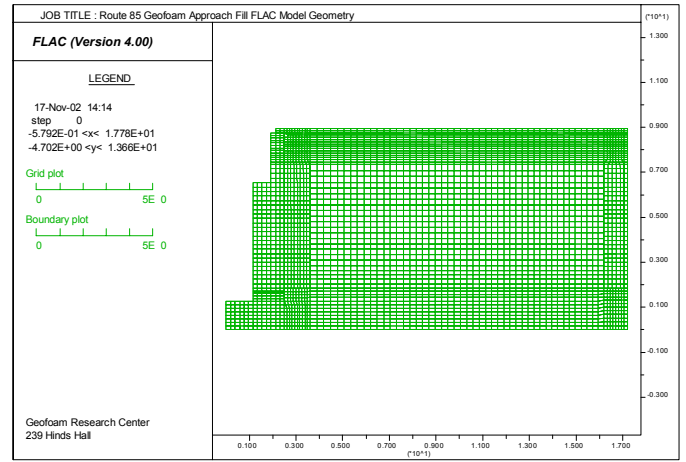
Fig. 11. Element grid for FLAC modeling of the Route 85 geofoam approach fill.
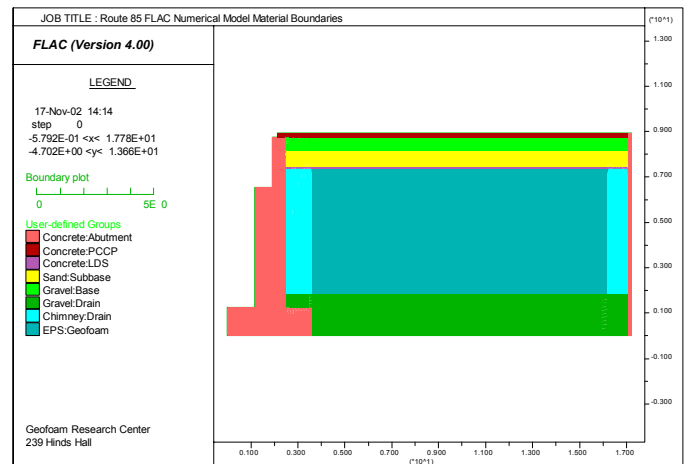
Fig. 12. Material boundaries for FLAC model for the Route 85 geofoam approach fill.

A constitutive model for geofoam under confinement was proposed by Preber et al. (1994) based on triaxial test results on geofoam samples for densities ranging from 16 to 32 kg/m^3 and confining stresses of 0 to 62 kPa. The stress-strain equations presented by Preber et al. are:

$$\sigma = (I + E_p\varepsilon)[1 - \exp(-C\varepsilon^2 - \frac{E_i\varepsilon}{I})] \qquad (2)$$

$$C = -\frac{E_i}{IX_o} - \frac{1}{X_o^2}\ln[1 - \frac{Y_o}{(I + E_pX_o)}] \qquad (3)$$

where: σ = axial stress

ε = axial strain

E_i = initial modulus

E_p = post-yield modulus

I = axial stress at intersection of stress axis and plastic tangent

X_o = strain at intersection of elastic and plastic tangent

Y_o = stress at intersection of elastic and plastic tangent

Material	ρ (kg/m³)	K (Pa)	G (Pa)	φ (°)	K_N (Pa/m)	K_S (Pa/m)	Material Model
			Material Parameter				
Abutment/LDS/PCC Approach Slab	2530	1.4×10^{10}	1.17×10^{10}	-	-	-	Elastic
Subgrade	1600	1.67×10^{7}	1.0×10^{7}	32	-	-	Mohr-Coulomb
Gravel Drain	1700	2.67×10^{7}	1.6×10^{7}	34	-	-	Mohr-Coulomb
Chimney Drain	1750	2.4×10^{7}	1.1×10^{7}	34	-	-	Mohr-Coulomb
Sub-Base	1850	2.4×10^{7}	1.1×10^{7}	34	-	-	Mohr-Coulomb
Base	1900	2.67×10^{7}	1.6×10^{7}	34	-	-	Mohr-Coulomb
HMA	2350	3.9×10^{9}	1.3×10^{9}	-	-	-	Elastic
Geofoam, $E_I = 4.1$ MPa, $\nu = 0.3$	18.5	3.4×10^{6}	1.58×10^{6}	-	-	-	Hyperbolic
Geofoam, $E_I = 4.1$ MPa, $\nu = 0.2$	18.5	2.28×10^{6}	1.71×10^{6}	-	-	-	Hyperbolic
Geofoam, $E_I = 11$ MPa, $\nu = 0.3$	18.5	9.17×10^{6}	4.23×10^{6}	-	-	-	Hyperbolic
Geofoam, $E_I = 11$ MPa, $\nu = 0.2$	18.5	6.11×10^{6}	4.58×10^{6}	-	-	-	Hyperbolic
Geofoam/Geofoam Interface	-	-	-	31	4×10^{7}	2.9×10^{7}	-
Chimney Drain/Geofoam Interface	-	-	-	31	4×10^{8}	2.9×10^{8}	-
Gravel Drain/Abutment Interface	-	-	-	34	5.5×10^{10}	3.5×10^{10}	-
Chimney Drain/Abutment Interface	-	-	-	34	5.5×10^{10}	3.5×10^{10}	-
LDS/Abutment Interface	-	-	-	23	2.75×10^{11}	1.75×10^{11}	-
Sub-Base Interface	-	-	-	34	5.5×10^{10}	3.5×10^{10}	-
Chimney Drain/Lagging Wall Interface	-	-	-	31	1.82×10^{10}	1.27×10^{10}	-
Base/Abutment Interface	-	-	-	34	5.5×10^{10}	3.5×10^{10}	-

Table 2. Material properties for FLAC numerical models

Preber et al. used the following expressions to generate the equations for expressing geofoam behavior with respect to confining stress:

$$I = (-107 + 910\gamma) + (0.63 - 6.32\gamma)\sigma_3 \quad (4)$$

$$E_i = (-4{,}180 + 39{,}000\gamma) + (-6.2 - 53\gamma)\sigma_3 \quad (5)$$

$$E_p = (85.5 + 638\gamma - 403\gamma^2) + (-3.4 + 28.4\gamma)\sigma_3 \quad (6)$$

$$Y_o = (-119.4 + 924\gamma) + (0.962 - 7.5\gamma)\sigma_3 \quad (7)$$

$$X_o = \frac{I}{(E_i - E_p)} \quad (8)$$

where: σ_3 = confining stress, kPa
 γ = unit weight, kN/m³

Compressive strengths at 5% strain returned from the above equations are approximately 25% lower than reported by Sun (1997). Anasthas (2001) performed a series of triaxial compression tests on geofoam samples of 16 to 26 kg/m³

density and confining pressures of 0 to 100 kPa. The following equations were proposed by Anasthas (2001) to express initial and post-yield modulus:

$$E_i \text{ (MPa)} = 0.0001\rho\sigma_3 + 0.008\rho^2 + 0.152\rho + 0.015 - 0.041\sigma_3 + 0.00006\sigma_3^2 \quad (9)$$

$$E_p \text{ (kPa)} = -0.01\rho\sigma_3 - 0.051\rho^2 + 9.566\rho + 0.966 + 1.812\sigma_3 - 0.005\sigma_3^2 \quad (10)$$

Replacing equations (5) and (6) with (9) and (10) for use in (2) and (3), the stress-strain behavior of geofoam is better predicted. The resulting equations (2) and (3) constitute modifications to equations proposed by Preber et. al (1994).

The hyperbolic model, provided in FLAC was adapted to represent the stress-strain behavior of geofoam as:

$$\sigma_d = \frac{\varepsilon}{\dfrac{1}{E_i} + \dfrac{\varepsilon}{Y}} \quad (11)$$

where: $\sigma_d = |\sigma_1 - \sigma_3|$
  ε = axial strain
  Y = maximum value of $|\sigma_1 - \sigma_3|$
  E_i = initial Young's modulus

Y and E_i are derived from equations (2) and (9) for an appropriate density and confining stress conditions. Both the Preber et al and hyperbolic representations of geofoam behavior capture the distinct trends of strength and modulus degradation with increasing confining stress levels, as shown in Fig. 13 for confining stresses of 0 and 35 kPa.
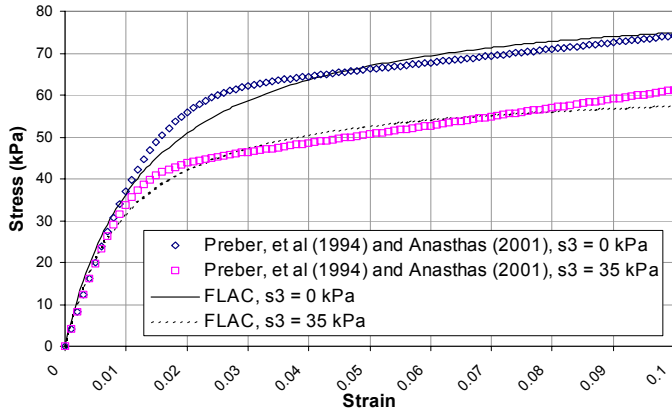

Fig. 13. Comparison of stress-strain results for geofoam under confinement, modified Preber et al and hyperbolic equations.

A parametric study was conducted to investigate the relative sensitivity of the model to changes in geofoam initial modulus and Poisson's ratio. Compressive tests on small, 50 mm cube samples for EPS 20 resulted in Young's modulus of 2.9 to 5.1 MPa for geofoam used on the Interstate-15 Reconstruction Project (Bartlett, et al., 2001; Negussey et al., 2001). Further studies (Duskov, 1997; Elragi, 2000; Anasthas, 2001; Sivathayalan, et. al, 2001; Stuedlein, 2003) have shown the Young's modulus of EPS 20 to be larger by a factor of over 2 when evaluated utilizing large samples and localized observations of deformations. Further, Srirajan (2001) indicated Poisson's ratios for geofoam generally range from 0.2 to 0.3. Trial designations and corresponding parameters for the investigation are given in Table 3.

Table 3. Parameters investigated with FLAC models.

Model Trial Number	Initial Modulus (MPa)	Poisson's Ratio
1	4.1	0.2
2	4.1	0.3
3	11	0.2
4	11	0.3

COMPARISON OF FIELD AND MODEL RESULTS

The FLAC model results represent the Route 85 project at the end of construction. Long-term performance was not simulated as part of this investigation. The field observations used for comparison of numerical model results correspond to

the time period where the approach slab had been in place for a month and the hot-mix asphalt had been laid. Table 4 shows the comparison of field observations from the magnet extensometers and the model results. Better agreements were obtained for Trials 3 and 4, both of which use the higher Young's modulus. Figure 14 shows the geofoam displacement from field and model results for Trial 4. The agreement between the model results and field settlement observations is better for the global geofoam fill, all six layers, in contrast to only the first two layers.

Table 4. Comparison of geofoam fill strain.

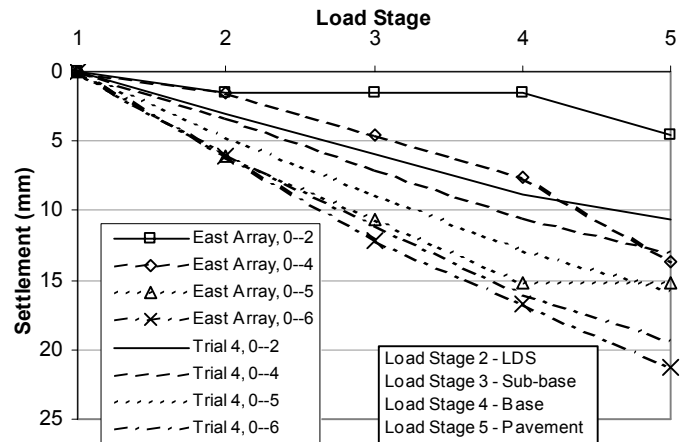| Source	Strain at Magnet Extensometer Location	Maximum Geofoam Strain
East Array	0.0039	-
West Array	0.0045	-
1	0.0070	0.0086
2	0.0055	0.0068
3	0.0042	0.0048
4	0.0035	0.0037

Fig. 14. Comparison of settlements and FLAC model Trial 4, using Young's modulus of 11 MPa and Poisson's ratio of 0.3.

Base stresses observed at the bottom of the geofoam fill are compared against predictions from the numerical modeling, Table 5. All trials overestimate stresses observed at the end of construction. The load history of the foundation for the new bridge construction is mixed, with pre-loading from the existing embankment side slopes in the area of the West Array as opposed to virgin loading of the foundation on the East Array. With differential movements of the fill and pile supported abutment and wing walls, interaction effects and transfer of vertical loads may be occurring. Foundation settlements below the geofoam fill are not represented in the FLAC models. Nevertheless, both the model and observed stresses amount to less than about 20 percent of geostatic stresses for a compacted earth approach fill.

Vertical and horizontal stresses observed in the chimney drain between the abutment and geofoam are compared with the FLAC model results in Fig.'s 15, 16, and 17. The vertical chimney drain incremental stresses show good agreement in trend, although the magnitude of stresses is over predicted in all numerical models. When considering the free field one-dimensional stress estimate of 135 kPa (top dashed line in Fig. 15) at the bottom of the drain, the numerical models provide much better comparison. Trial 3, using the high Young's modulus and lower Poisson's ratio of 0.2, best predicts the lateral stresses. All model trials under predict the lower (PC 4H, Fig. 16) lateral stresses in the early stages of loading and over predict by the end of construction. Model trials over predict observations in all cases for the upper (PC 5H, Fig. 17) lateral stress cell within the chimney drain fill. For both the upper and lower stress cell positions, model results and observations are much less than lateral pressures that may be expected to be induced by action of equivalent surcharge overlying earth rather than geofoam fill.

SUMMARY AND CONCLUSIONS

The new Route 85 bridge across Normans Kill was completed while the old bridge remained in service. Use of EPS geofoam allowed portions of the new approach fill to be constructed over virgin foundation soils without inducing detrimental settlements to the old bridge. The bridge construction required less time and partly occurred in winter. Field observations indicate the geofoam approach fill performance to date is satisfactory and the long-term performance continues to be monitored. With suitable constitutive relations, FLAC model results show reasonably good agreement with field observations. Conclusions from this study include:

1) The EPS geofoam fill produced about 0.5 percent strain over the course of construction. Total strain of about 0.8 percent has been registered to date.
2) Use of granular drain materials between geofoam fills and abutments or wing walls likely resulted in soil arching.
3) Deformation estimates based on parameters derived from testing small. geofoam samples would tend to over predict settlements.
4) Numerical models incorporating higher Young's modulus of 11 MPa and Poisson's ratio of 0.2-0.3 resulted in good agreement with field performance of EPS 19 geofoam.
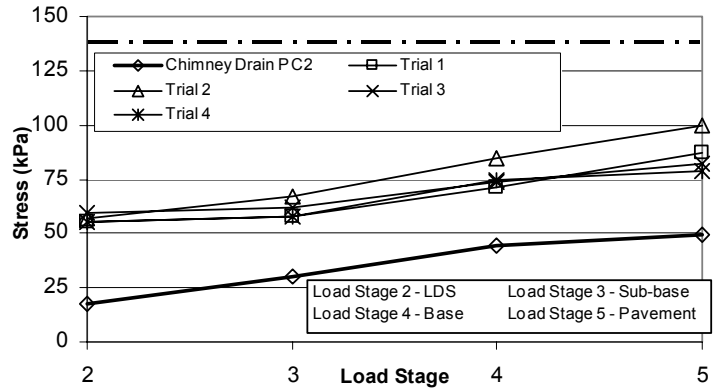
ACKNOWLEGMENTS

Fig. 15. Comparison of observed and modeled vertical chimney drain stresses.
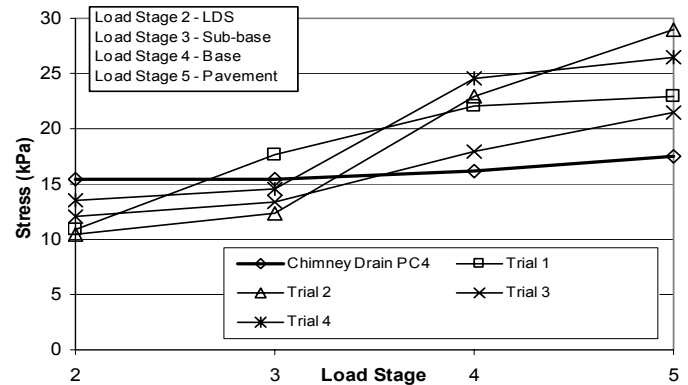

Fig. 16. Comparison of observed and modeled lateral chimney drain stresses for lower (PC4) stress cell location.
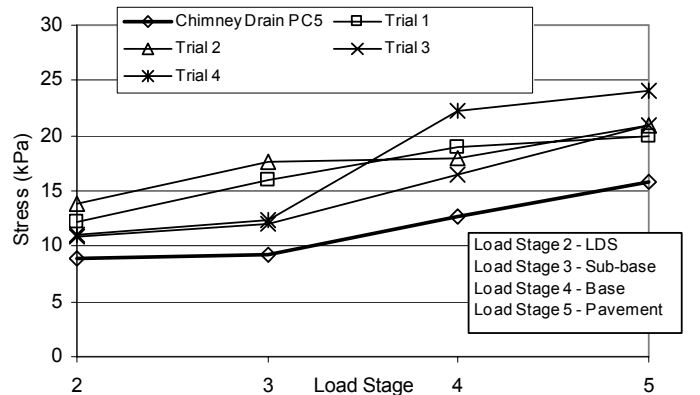

Fig. 17. Comparison of observed and modeled lateral chimney drain stresses for upper (PC5) stress cell location.

Table 5. Comparison of observed and modeled end of construction vertical stresses below the geofoam fill.

Source	PC 1V East Array Stress (kPa)	PC 3V West Array Stress (kPa)
Stress Cells	3.5	15.5
1	21.7	26
2	24.8	24
3	25	22
4	24.5	24

REFERENCES

Anasthas, N. [2001]. *"Young's Modulus By Bending Test and Other Properties of EPS Geofoam Related to Geotechnical Applications",* M.S. Thesis, Syracuse University, Syracuse, NY

Arai, N., Yokoyama, M., and Tamura, H. [1996]. *"EPS Embankment Construction Road For 32 Ton Dump Trucks At Gassan Dam",* EPS Tokyo '96, Proceedings of the 2nd International Symposium on EPS Construction Method, Tokyo

Bartlett, S., Farnsworth, C., Negussey, D., and Stuedlein, A. W. [2001]. *"Instrumentation and Long-Term Monitoring of Geofoam Embankments, I-15 Reconstruction Project, Salt Lake City, UT",* Proceedings of EPS 2001, 3rd International Conference of EPS Geofoam, Salt Lake City, UT

Druss, D. L., Bobrow, D., Peterson, J., and Beale, R. [1998]. *"Geotechnical Instrumentation for a Megaproject",* Design and Construction of Earth Retaining Systems, Geotechnical Special Publication No. 83, pp. 63-81; Finno, R. J., Hashash, Y., and Sweeney, B., Eds.; ASCE, New York

Duškov, M. [1997]. *"EPS as a Light-Weight Sub-base Material in Pavement Structures",* Ph.D. Thesis, Delft University of Technology, Delft, The Netherlands

Elragi, A. F. [2000]. *"Selected Engineering Properties and Applications of EPS Geofoam",* Ph.D. Thesis, State University of New York, Syracuse, NY

Handy, R., L. [1985]. *"The Arch in Soil Arching",* Journal of Geotechnical Engineering, Vol. 111, No. 3, ASCE, New York,

Munfakh, G., A., Sarkar, S. K., and Castelli, R. J. [1983]. *"Performance of a Test Embankment Founded on Stone Columns",* Proceedings of the Symposium on Advances in Piling and Ground Treatment for Foundations, Institution of Civil Engineers, London

Negussey, D., Stuedlein, A. W., Bartlett, S. F., and Farnsworth, C. [2001]. *"Performance of a Geofoam Embankment at 100 South, I-15 Reconstruction Project, Salt Lake City, UT",* Proceedings of EPS 2001, 3rd International Conference of EPS Geofoam, Salt Lake City, UT

O'Rourke, T. D., and O'Donnell, C. J. [1997]. *"Field Behavior of Excavation Stabilized by Deep Soil Mixing",* Journal of Geotechnical and Geoenvironmental Engineering, Vol. 123, No. 6, ASCE, New York

O'Rourke, J. E. [1978]. *"Soil Stress Measurement Experiences",* Journal of Geotechnical Engineering, Vol. 104, No. 12, ASCE, New York

Preber, T., Bang, S., Chung, Y., and Cho, Y. [1994]. *"Behavior of Expanded Polystyrene Blocks",* Transportation Research Record 1462, Transportation Research Board, Washington D. C.

Saye, S. R., Esrig, M. I., Williams, J. L., Pilz, J., and Bartlett, S. F. [2001]. *"Lime Cement Columns for the Reconstruction of Interstate 15 in Salt Lake City, Utah",* Foundations and Ground Improvement, Proceedings of Geo-Odyssey 2001, Geotechnical Special Publication No. 113, Brandon, T. L., Ed.; ASCE, New York

Sivathayalan, S., Negussey, D., and Vaid, V. P. [2001]. *"Simple Shear and Bender Element Testing of Geofoam",* Proceedings of EPS 2001, 3rd International Conference of EPS Geofoam, Salt Lake City, UT

Srirajan, S. [2001]. *"Recycled Content and Creep Behavior of EPS Geofoam in Slope Stabilization",* M.S. Thesis, Syracuse University, Syracuse, NY

Stuedlein, A. W. [2003]. "*Instrumentation, Performance, and Numerical Modeling of Large Geofoam Embankment Structures",* M.S. Thesis, Syracuse University, Syracuse, NY

Slope Indicator, Inc. [2002]. *"Digitilt Inclinometer Probe",* Bothell, WA

Sun, M. C. [1997]. *"Engineering Behavior of Geofoam (Expanded Polystyrene) and Lateral Earth Pressure Reduction in Substructures",* M.S. Thesis, Syracuse University, Syracuse, NY

Weiler, W. A., and Kulhawy, F. H. [1978] *"Behavior of Stress Cells in Soil",* Contract Report B-49(4), to Niagara Mohawk Power Corp., Cornell University, Ithaca, NY